Easy Synthesis and Imaging Applications of Cross-Linked Green Fluorescent Hollow Carbon Nanoparticles

Youxing Fang, Shaojun Guo, Dan Li, Chengzhou Zhu, Wen Ren, Shaojun Dong, and Erkang Wang*

State Key Laboratory of Electroanalytical Chemistry, Changchun Institute of Applied Chemistry, Chinese Academy of Sciences, Changchun 130022, Jilin, People's Republic of China, and Graduate School of the Chinese Academy of Sciences, Beijing 100039, People's Republic of China

ABSTRACT

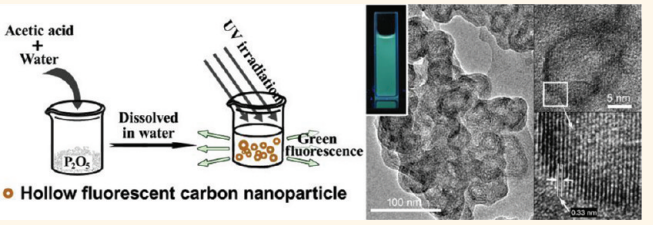

We propose an ingenious method for synthesizing cross-linked hollow fluorescent carbon nanoparticles (HFCNs) with green emission by simply mixing acetic acid, water, and diphosphorus pentoxide. This is an automatic method without external heat treatment to rapidly produce large quantities of HFCNs, in contrast to other syntheses of fluorescent carbon nanoparticles that required high temperature, complicated operations, or long reaction times. Characterizations of HFCNs through high-resolution transmission electron microscopy, infrared/Raman spectroscopy, and X-ray diffraction indicate that abundant small oxygenous graphite domains existed and endowed the HFCNs with fluorescent properties. After simple post-treatments, the cross-linked HFCNs can be used for cell-imaging applications. Compared with traditional dyes and CdTe quantum dots, HFCNs are the superior fluorescent bioimaging agent according to their low toxicity, stability, and resistance to photobleaching. The HFCNs were also applied to watermark ink and fluorescent powder, showing their promising potentials for further wide usage.

KEYWORDS: fluorescent carbon nanoparticle · one-step synthesis · hollow nanoparticles · fluorescent bioimaging

Fluorescent carbon nanoparticles (FCNs) are attracting considerable attention because of their potential applications in bioimaging,[1,2] photocatalysis,[3,4] and light-emitting devices.[5] As an alternative for fluorescent chalcogenide semiconductor nanocrystals (QDs), FCNs are superior fluorescent nanomaterials with low toxicity, high chemical stability, and low environmental hazard.[6] FCNs are generally small oxygenous carbon nanoparticles (<10 nm) and could be classified as the new zero-dimensional member in the versatile carbon nanomaterial family. With the exception of nanodiamonds, most FCNs are composed of sp^2 carbon atoms hybridized with abundant oxygenous residues, which induce small conjugated carbon clusters (aromatic structures) embedded in oxygenous groups. The isolated aromatic structures[6,7] (otherwise, the carbenes[8] stabilized by aromatic structures at the zigzag sites) possess suitable band gaps, and radiative recombination would generate visible fluorescence of the FCNs. Although their intrinsic mechanism of fluorescence is not yet clearly understood, the environmentally benign FCNs have been prepared by the arc-discharge method,[9] laser ablation of graphite,[1,10−12] decomposition of diverse carbon sources,[3,13−32] ion-beam irradiation of nanodiamonds,[33,34] carrier methods,[35−37] and microwave synthesis.[38] However, the above methods may involve severe synthetic conditions, long consumption time, low available amounts, and inconvenient postsynthetic treatments. Thus, developing a simple and convenient way for the preparation of FCNs remains highly desirable before energy-saving techniques are carried out on a large scale for commercial usage.

As large-sized carbon nanoparticles have poor or no fluorescent emission, the general difficulty in synthesizing FCNs is to maintain the small size of the carbon component. Manufacturing and refining small carbon fragments, "carbon dots", is commonly adopted to address this issue according to the aforementioned methods. Due to their small size, the synthesis of carbon dots brings additional barriers to simplify the tedious post-treatment as well as increase the reaction yield. Moreover, FCNs with other morphologies (such as hollow and core−shell structures) may be rightfully obtained as long as the carbon component fits the size request, which might broaden both the "dot" concept and their cooperation with other

* Address correspondence to ekwang@ciac.jl.cn.

Received for review September 29, 2011 and accepted December 21, 2011.

Published online December 21, 2011
10.1021/nn2046373

species for diverse potential functional materials based on FCNs. In this work, an ingenious strategy was utilized to keep the carbon components small by yielding hollows during the carbonation reaction. So that the as-prepared FCNs with hollow interiors are notated as HFCNs. The cross-linked HFCNs with green emission were rapidly produced by mixing acetic acid (AC), water, and diphosphorus pentoxide (P_2O_5). The synthesis can be termed as a bottom-up and wet-chemical method because AC acts as both the polar solvent and the carbon precursor. The HFCNs are specifically obtained under self-generated heat. Various characterizations indicate that the HFCNs have small oxygenous graphite domains, which endow them with fluorescent emission. Interestingly, solid fluorescent carbon nanoparticles (SFCNs), which are obtained by solely reducing the released heat, served as the important benchmark toward HFCNs.

Modern diagnosis and therapy have been raising increasing demands toward fluorescent bioimaging agents with preferable properties, such as low toxicity, high stability, high fluorescent efficiency, and tunable excitation/emission windows. Although organic dyes are often used, their poor photostability restricts their applications for long-term observation. On the other hand, QDs have received significant attention because they possess quite a few of merits including high fluorescent efficiency, broad excitation, and narrow and symmetric emission, which are well suited for simultaneous multicolor labeling and detection.[39−41] However, the usage of heavy metals causes serious problems due to their high biotoxicity,[42,43] and chalcogenides may also suffer from their low chemical stability toward photooxidation.[44] To overcome the drawback of heavy metal leaching, coated/immobilized QDs could be adopted to survive the cells.[45] Various materials, such as chitosan,[46] polyisoprene,[47] amphiphilic polymers,[48] poly(lactide-*co*-glycolide),[49] silica,[50] zirconia,[51] and proteins,[52,53] have been used to wrap the QDs. Nevertheless, the modified QDs need complicated synthesis routes, while the layer coated on QDs may not completely stop the decreased leaching of the heavy metals. FCNs, composed of carbon and oxygen (with or without nitrogen), can act as good candidates to circumvent the above problems.[2,31,33,35] Herein, cross-linked HFCNs were used as new fluorescent materials for cell imaging, taking CdTe QDs and dyes as the controls. The HFCNs have shown superior fluorescence stability under laser irradiation in contrast to CdTe QDs and dyes. Furthermore, two extended uses of HFCNs (fluorescent watermark ink and fluorescent powder) have been explored, indicating the diverse potential applications of these HFCNs.

RESULTS AND DISCUSSION

One milliliter of glacial AC containing 80 μL of water was quickly added to 2.5 g of P_2O_5 to produce HFCNs

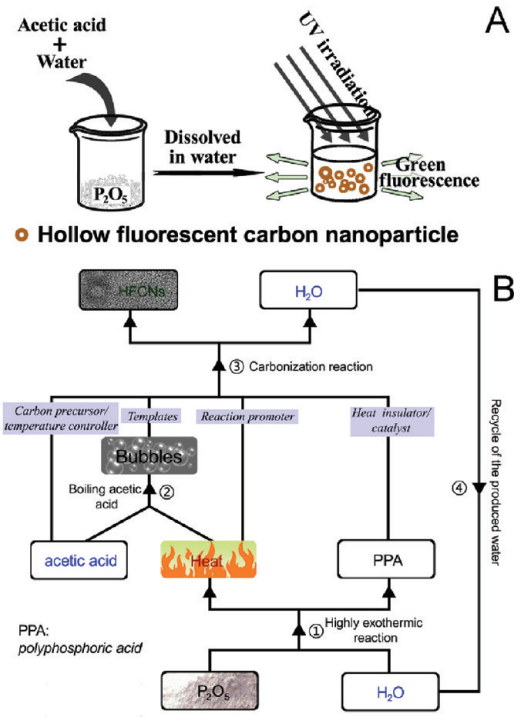

Figure 1. Synthetic method (A) and reaction process (B) yielding the HFCNs.

(Figure 1A). The color of the mixture changed to brown within 10 s, and the volume of the sticky slurry mixture was dramatically expanded by foaming because of the boiling of AC by the spontaneous heat. The reaction lasted for about 5 min until exhaustion of the P_2O_5 (Figure S1, Supporting Information (SI)). The elemental analysis of the crude product revealed that the carbonation rate was about 33.4% in the one-pot synthesis, and the carbonation product was calculated to be 0.14 g (counted by C element). We also measured the weight of HFCNs that was extracted by ethyl acetate, which is up to 0.063 g in the one-pot synthesis. At the same time, SFCNs were also produced by use of the same reactants. Compared to the synthesis of SFCNs with low efficiency, a huge volume of HFCN solution can be obtained within 10 min (Figure S2, SI). The automatic reaction is cost-effective to synthesize HFCNs without external heating. The self-engendered nanobubbles were produced to remove the excessive heat and utilized as the templates to restrict the size of the carbon component by creating hollow interiors. A diagram is shown in Figure 1B for the brief presentation of the whole reaction process, and details of fractional parts are interpreted below.

Choosing Carbon Precursors. The carbonization process involves three starting substances. Each of the three substances (AC, water, and P_2O_5) plays a very important role in the self-catalytic reaction, and AC was particularly selected as the carbon precursor. AC acts as both the oxygenous carbon resource and the hydrophilic reaction medium, which induces oxygenous

defects and good solubility for the HFCNs just like citric acid and glucose.[20,23,24] However, citric acid and glucose were not employed as carbon precursors in this synthesis for the following two reasons. (1) Solid-state carbon precursors may be initially dissolved in relatively large amounts of water for the carbonization reaction, while the diluted carbon precursor can affect the synthesis yield. (2) Most importantly, solid carbon precursors cannot limit the reaction temperature by themselves because of their relative high boiling points. In this system, the upper temperature was mainly controlled by vaporizing the AC at its boiling point (117 °C). Vaporization would remove the excessive heat, and the nanobubbles of AC vapor then served as the templates for hollow structures. Therefore, AC could restrict the size of nanostructured graphite *via* two spontaneous ways: limiting the reaction temperature and creating hollows by its physical nature. When the upper temperature limit was adjusted to 78.4 and 290 °C by changing the liquid carbon precursor to ethyl alcohol and glycerin with different boiling points, the carbonization reaction was hardly promoted at such a low temperature, whereas the higher temperature, leading to a high degree of graphitization, decreases the yield of soluble and fluorescent product (data not shown).

$$H_2O + \frac{n}{m}P_2O_5 \rightarrow \frac{1}{m}[(P_2O_5)_n \cdot H_2O_m] \quad (1)$$

$$CH_3COOH \xrightarrow[\Delta]{P_2O_5,\ PPA} 2C_{(HFCN)} + 2H_2O \quad (2)$$

Self-Heating. In the self-catalytic reaction, water is closely related to the released heat of the system. A trace amount of water was first introduced to the system, and it quickly reacted with P_2O_5 (eq 1). This reaction is highly exothermic, and the released heat was utilized to promote the carbonization reaction besides vaporizing the AC. Figure S1B (SI) shows a digital photograph of a reacting mixture. The self-heated mixture was greatly foamy because of the boiling AC. Continuous heat was produced, as the water was replenished by the carbonization reaction (eq 2). Sufficient water brings more heat to produce HFCNs. If the initial amount of water was decreased, insufficient heat could produce only SFCNs due to the lack of bubbles for hollow structures.

Autocatalysis. High chemical energy was converted to thermal energy along with P_2O_5 turning into phosphoric acid. In addition to its ability to react with free water, P_2O_5 is also very effective in removing *composite water*[54] from many organic and inorganic compounds.[55] Hence P_2O_5 as the dehydrating agent could accelerate the carbonization reaction according to eq 2. Excess P_2O_5 reacted with water to produce polyphosphoric acid (PPA).[55] PPA is the semihydrolyzed product of P_2O_5 and still maintains a strong dehydrating effect before its conversion to monophosphoric acid. Previous work also found that polyphosphate can promote the carbonation reaction at low temperature.[56] Moreover, PPA has two valuable physical properties in this system: high viscosity and relatively low melting point.[57] At 117 °C, the melted PPA dilutes AC by forming a liquid mixture of PPA and AC. Highly sticky liquid PPA captures the hot gas of AC to suppress the heat loss. Due to the above catalysis by both PPA and P_2O_5, the carbonization reaction starts and continues at 117 °C (measured by a thermometer in the reaction beaker). Overall, the synthetic process of HFCNs was controlled by a series of spontaneous conditions, such as relatively low temperature with an upper limit, bubbles, continuous heat, and catalysts. Meanwhile, the well-mixed reactants with the aid of boiling do not require stirring, which is another advantage of this synthesis.

After simple post-treatments, the HFCNs were collected for different characterizations. Figure 2A shows the typical transmission electron microscopy (TEM) images of the as-prepared cross-linked HFCNs at low magnification. It is seen that the HFCNs have bright centers. A high-resolution TEM (HRTEM) image (Figure 2B) shows the empty capacity of the HFCN. The shell thickness is less than 5 nm, which fits the previous reports of FCNs.[6] The well-defined crystal lattice (0.33 nm) of the HFCNs is shown in Figure 2C, being in agreement with the basal spacing of graphite. It should be noted that the HFCNs were cross-linked with each other, and a series of TEM images of cross-linked HFCNs are shown in Figure S3 (SI). Although it is difficult to compile statistics of the thicknesses of carbon shells from TEM images, the carbon shells are very thin (<5 nm). A TEM image of the SFCNs is displayed in Figure 2D. The SFCNs are all without bright centers. The SFCNs are synthesized *via* a similar procedure by insufficient spontaneous heat, resulting in no bubbles created by the boiling AC. The sizes of graphite nanodomains in SFCNs are also less than 10 nm; hence the SFCNs also possess fluorescent properties like the HFCNs. Two detailed images of individual HFCNs and SFCNs were separately collected, as shown in Figure S4 (SI), clearly showing the morphology differences between the hollow and solid products. We then characterized the size distributions by the dynamic light scattering measurement, and the overall sizes of HFCNs and SFCNs are 105 and 141 nm (Figure S5, SI), respectively. These results further corroborate that the HFCNs and SFCNs are linked with each other to form larger nanoparticles, suggesting this automatic synthetic method of FCNs preferably produces cross-linked carbon nanodomains.

Introducing hydrophilic groups to FCNs is a general protocol to improve the solubility of the FCNs, as well as isolate graphite nanodomains to induce fluorescent properties. By use of AC as the carbon source with a

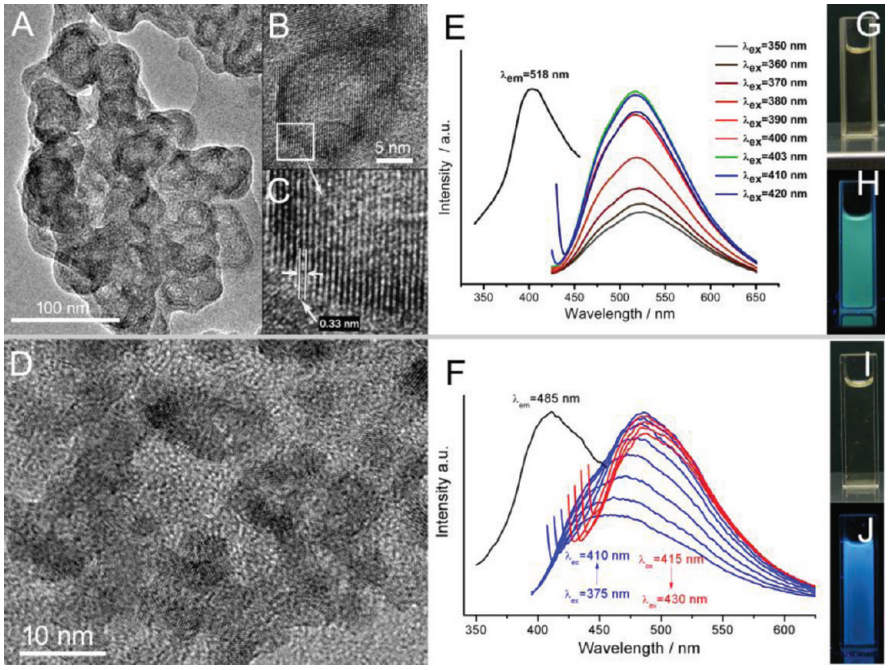

Figure 2. TEM images of HFCNs (A–C) and SFCNs (D). Fluorescent spectra of the HFCNs (E) and SFCNs (F) in PPA solution. HFCNs (G, H) and SFCNs (I, J) under room light (G, I) and UV light (H, J; 365 nm).

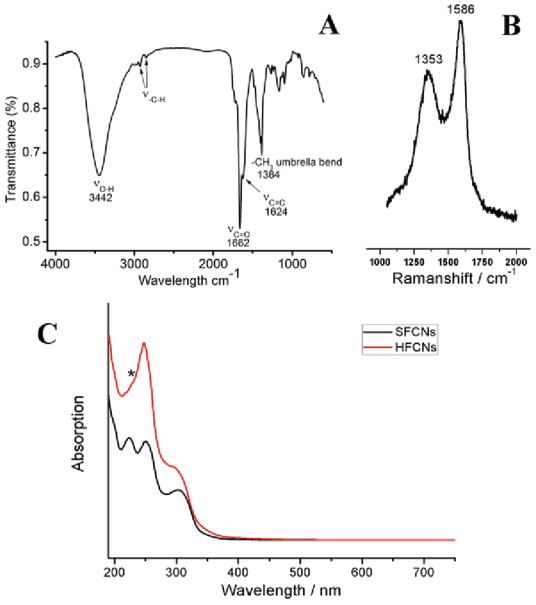

Figure 3. Typical FT-IR (A) and Raman spectrum (B) of HFCNs. Absorption spectrum (C) of SFCNs and HFCNs.

carboxylic group, this method directly results in oxygenous defects and water solubility of HFCNs. Figure 3A shows the FT-IR spectrum of the HFCNs, where an apparent absorption peak of the −OH group at about 3442 cm^{-1} and an absorption peak of the C═O group conjugated with condensed aromatic carbons at 1662 cm^{-1} appear, respectively. These data reveal that the obtained HFCNs are rich in carboxylic groups. In addition, a negative zeta potential of the HFCNs was recorded (−12.6 mV) in aqueous solution, corroborating the presence of residual carboxylic groups at their surface. The conjugated sp^2 carbon has been verified by various spectroscopies. A peak at 1624 cm^{-1} arising from a conjugated C═C stretching vibration was observed in the FT-IR spectrum, indicating unsaturated carbon bonds are formed during the carbonization process. The ^{13}C nuclear magnetic resonance of HFCNs (Figure S6, SI) shows three kinds of carbon peaks around the three regions:[58] 20–30 ppm (residual sp^3 carbon atoms); 100–150 ppm (sp^2 carbon atoms, C═C); 150–210 ppm (sp^2 carbon atoms; C═O), in accordance with the related observation according to the FT-IR results. The unsaturated carbon bonds were further confirmed by the Raman spectrum. In Figure 3B, the peak at 1586 cm^{-1} (G band) is associated with the E_{2g} mode of the graphite and is related to the vibration of sp^2-bonded carbon atoms in a two-dimensional (2D) hexagonal lattice. The D band at around 1353 cm^{-1} is ascribed to the vibrations of carbon atoms with dangling bonds in the termination plane of disordered graphite or glassy carbon.[3,59–62] A broad G peak of HFCNs (~100 cm^{-1}, full width at half-maximum) was observed, and the size of graphite nanodomains (<5 nm) could be estimated, as the decreasing sp^2 grain size leads to the wide G band peak.[63] The intensity ratio (I_D/I_G), which is often used to correlate the structural purity to the graphite, also reveals that the HFCNs are mainly composed of nanocrystalline graphite.[31,64] The average integrated intensity ratio of the D and G bands was calculated to be larger than 2.0 from three individual batches of HFNCs (Figure S7, SI), indicating that a small size of the nanocrystalline graphite was obtained.[64,65] The X-ray powder diffraction pattern of the HFCNs is displayed in

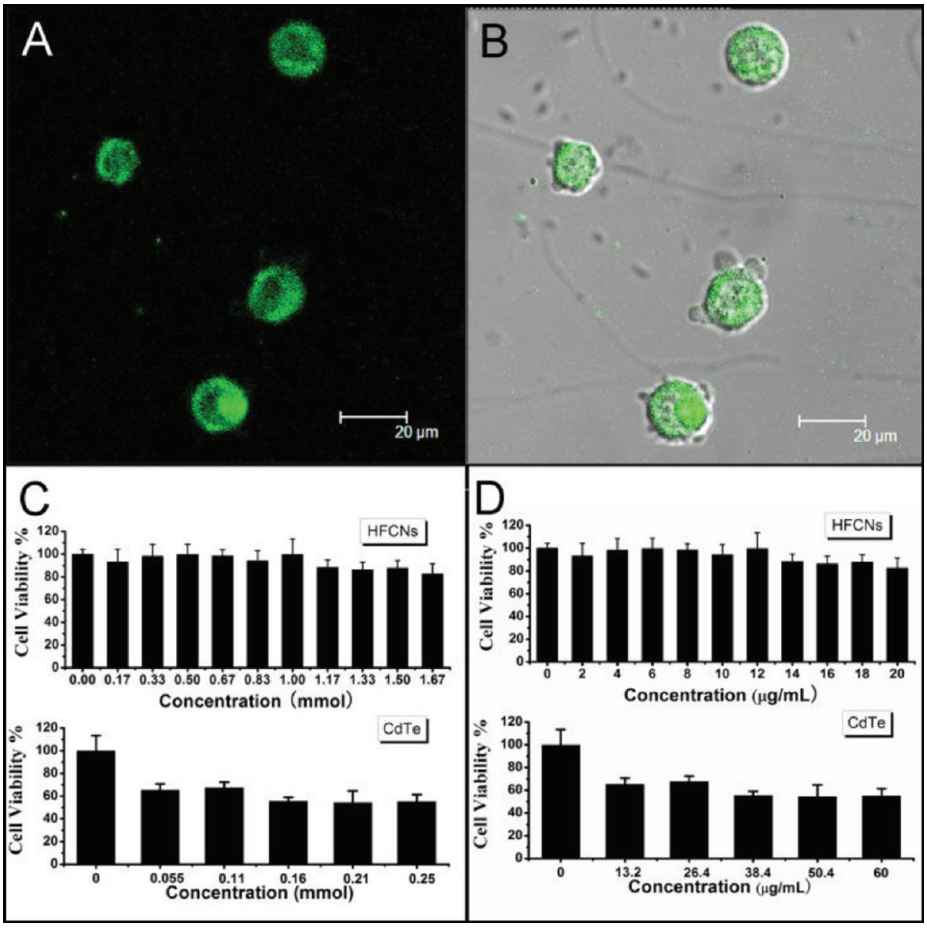

Figure 4. (A) CLSM images showing HFCNs in living HEK 293 cells (A) and overlay CLSM images and bright field of HEK 293 cells (B). Excitation: 405 nm. All scale bars represent 20 μm. Cytotoxicity tests of HFCNs (top) and CdTe QDs (bottom) based on molar (C) and weight (D) concentrations with HEK 293 cells.

Figure S8 (SI). Two wide reflection peaks of the (002) and (100) facets were observed, indicating the partial graphitization of the HFCNs. As was aforementioned, graphite structures have been determined by measuring basal spacing with HRTEM. Thus, the above analyses indicate that the graphitic nanodomains in HFCNs contain polyaromatic structures, which were probably isolated by the oxygenous groups. These isolated polyaromatic structures may serve as fluorescent chromophores and introduce fluorescence of HFCNs. Similarly, this luminescence mechanism could also be suitable for the SFCNs.

Figure 2E shows the typical fluorescent spectra of the HFCN after one-time centrifugation (8000 rpm, 5 min). The black curve is the excitation spectrum at 518 nm emission, and the other colorful curves are the emission spectra at excitations from 350 to 420 nm. Interestingly, the emission spectra of the HFCNs have no shift as the excitation wavelength varied, which is quite different from many previous reports[6] and the SFCNs we prepared. This phenomenon may be caused by fluorescence resonance energy transfer. The relatively small sized nanodomains of graphitic carbon emit blue light, which is in the range of fluorescence excitation of other larger nanodomains, and the HFCNs will finally yield green light under ultraviolet excitation (Figure 2H). Different from HFCNs, the SFCNs emit blue-green light under UV light (Figure 2J), and their fluorescent emission peaks gradually shift from ~450 to 500 nm as the excitation wavelength changes from 375 to 430 nm (Figure 2F). The difference in emission lights can be attributed to the different graphitization temperatures. Compared with SFCNs obtained at ~90 °C, HFCNs were produced at relatively higher temperature (117 °C) for a higher graphitization degree. Thus, HFCNs would achieve relatively larger graphite nanodomains and exhibit fluorescent emission at longer wavelengths. At the same time, nanobubbles suppress the excessive growth of graphite nanodomains in HFCNs, which may lead to the continuous red shifts of fluorescent emissions (even to no fluorescence) by much larger carbon components. This property of HFCNs lowers the demand of excitation light source to obtain invariable fluorescent emission, benefiting their further imaging applications.

The HFCNs and SFCNs are further characterized by UV–vis spectroscopy. In Figure 3C, a broad absorption around 300 nm and a sharp absorption at 247 nm were observed in absorption spectra of both HFCNs (red line) and SFCNs (black line). The peak at 247 nm is likely

originated from the formation of multiple polyaromatic chromophores,[33,34] while the broadened peak at 300 nm may be attributed to n–π* transitions of C=O.[7] Interestingly, an additional absorption at 223 nm was found from the UV–vis spectrum of the SFCNs, and the disappearance of this peak in the HFCNs can be interpreted as follows. In the carbonization reactions, the reaction temperature affects the degree of graphitization. A higher graphitization degree induces a red-shift of the fluorescence (in this work, from blue to green), resulting from the enhanced degree of π conjugation and the decreased band gaps. Similarly, some absorption wavelengths would be also red-shifted if they correlated with an enhanced degree of π conjugation. Thus, the peak at 223 nm could arise from the relatively small polyaromatic structures in SFCNs. This additional absorption peak of SFCNs finally shifted red and overlapped with the peak at 247 nm, and was hardly observed (asterisk in Figure 3C) in the absorption spectrum of HFCNs. However, the original peaks located at 300 and 247 nm may be attributed to other chromophores that are not associated with the influence of the enlarged polyaromatic structures.

Considering the facile preparation and interesting fluorescence of the present HFCNs, it is fascinating to explore whether HFCNs can be used as a new fluorescent marker for living cell imaging. Laser scanning confocal microscopy (LSCM) studies, shown in Figure 4A,B, suggest that the HFCNs without the modifier/surface-passivated agent have low cytotoxicity as bioimaging materials, and the cytotoxicity of HFCNs is further tested by MTT assay, taking CdTe (chalcogenide QDs) for comparison. Survival rates greater than 85% can be achieved in HFCNs-treated culture medium; however, comparable dosages of CdTe cause significant cell death, with survival rates between 65% and 55% (Figure 4C and D). Figure S9 (SI) shows the photostability of the HFCNs. No significant change of the fluorescent intensity was observed (>95% normalized intensity in 5000 s), indicating that these HFCNs display good photostability. We then compared the photostability of fluorescent materials (HFCNs, CdTe QDs, and the organic dye (fluorescein isothiocyanate (FITC), Hoechst)) for long-term cellular imaging. As shown in Figure 5A, the HFCNs-labeled cells are obviously detectable after 25 min, whereas the cells marked by CdTe QDs, FITC, and Hoechst are almost not observed

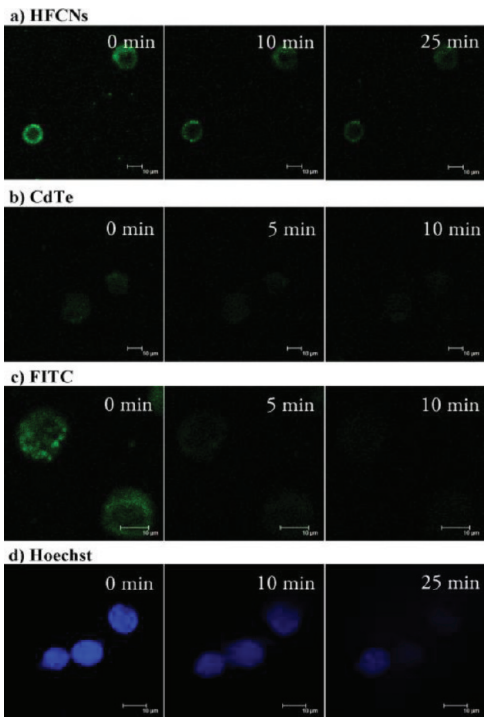

Figure 5. CLSM images showing time-dependent fluorescence signals of HEK 293 cells imaged by FCNs, CdTe QDs, FITC, and Hoechst. All scale bars represent 10 μm.

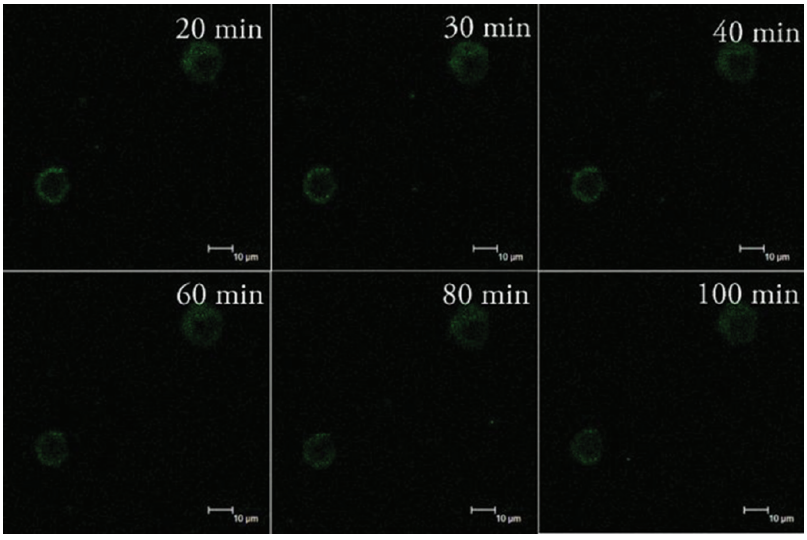

Figure 6. CLSM images showing time-dependent fluorescence signals of HEK 293 cells imaged by FCNs from 0 to 100 min. All scale bars represent 10 μm.

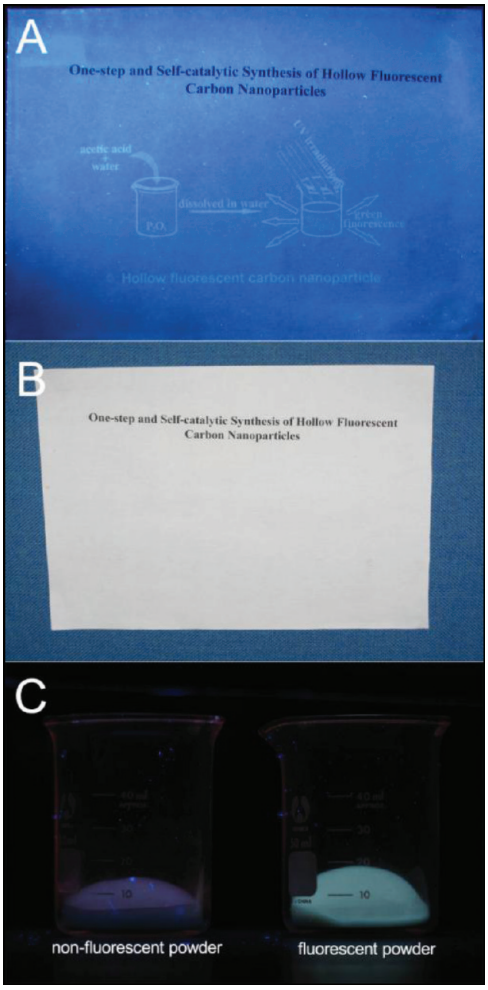

Figure 7. Digital photographs of the green diagram printed with HFCNs ink under 365 nm UV irradiation (A) and room light (B). The black text is printed by an ordinary printer. Digital photographs of silica powder loaded without (left) and with (right) HFCNs under 365 nm UV irradiation (C).

within 25 min under the same intensity of the laser excitation. Although CdTe QDs show bright fluorescence in aqueous solution, their toxicity is remarkable toward cells if they have not been wrapped or immobilized by innocuous materials. With prolonged irradiation time from 20 to 100 min, the green fluorescent signals of HFCNs are almost unchanged (Figure 6). These results suggest the HFCNs are a superior fluorescent bioimaging agent due to their low toxicity, stability, and resistance to photobleaching. The HFCNs, benefiting from their large-scale synthesis and low toxicity, are also available as a fluorescent agent for daily work. After simple post-treatments, the HFCNs have been used for fluorescent watermark ink and fluorescent powder. A digital photograph is shown in Figure 7A, and a diagram was clearly revealed under UV light. Furthermore, HFCNs can be loaded on commercial silica gel to obtain a fluorescent powder by vaporization of the solvent of ethyl acetic, a good solvent for HFCNs that extracts the HFCNs from the water solution. As seen (Figure 7C), the nonfluorescent silica powder (left) changes into a fluorescent-response power (right) just after adsorption of the HFCNs. Notably, the fluorescent properties of the above two products have been preserved for more than 3 months without significant changes. Therefore, the simple synthesis of HFCNs provides a new way to feed the potential requirement on a commercial scale.

CONCLUSION

In summary, we developed an ingenious strategy for fabrication of cross-linked HFCNs with green fluorescence. The synthesis of HFCNs is self-promoted and self-controlled by the chemical and physical properties of the reactants without any external treatment. When the self-released heat reaches the requirement of boiling AC, a considerable amount of HFCNs could be produced. Therefore, the carbonization reaction is an "automatic" synthesis of cross-linked HFCNs. In addition, insufficient self-released heat results in a few SFCNs, which serve as the appropriate reference for understanding the synthetic routes and fluorescent properties of HFCNs. The above investigations demonstrate the use of simple approaches to control the spontaneous reaction process, which prefers completely utilizing every property of the reactants, reactions, products, and byproducts. Moreover, characterizations through HRTEM, infrared/Raman spectroscopy, and X-ray diffraction indicated that the HFCNs have small oxygenous graphite domains, which endow them with fluorescent properties. This origin of the fluorescence may be further understood by the red-shifted fluorescent and absorption spectra of HFCNs, taking advantage of SFCNs as an important control. Finally, the as-prepared HFCNs can be efficiently post-treated by centrifugation, filtration, or extraction for several long-time imaging applications, from cell imaging in the laboratory to fluorescent marks in daily work. Through these usages of HFCNs, their superior low-toxicity and stability are clearly shown, in contrast to dyes and chalcogenide QDs. Thus, cross-linked HFCNs are promising fluorescent imaging agents with merits including their convenient and large-scale synthesis, stability, and low toxicity for potential applications.

MATERIALS AND METHODS

Materials. Glacial acetic acid, diphosphorus pentoxide, sodium hydroxide, cadmium chloride, and trisodium citrate dihydrate were obtained from Beijing Chemical Company (Beijing, China). Ethyl acetate was purchased from Sinopharm Chamical Reagent Co., Ltd. (Shanghai, China). Mercaptosuccinic acid, fluorescein isothiocyanate (FITC), and Hoechst 33342 were purchased from Aldrich. Sodium borohydride was purchased from Acros.

Na_2TeO_3 was bought from Schering-Kahlbaum in Germany. Water used throughout all experiments was purified with a Millipore system.

Preparation of HFCNs. A homogeneous mixture solution of glacial acetic acid (1 mL) and water (80 μL) was quickly added to 2.5 g of P_2O_5 in a 25 mL beaker without stirring. *Caution: This synthesis should be carried out in a fume hood to prevent inhaling acetic acid vapor!* The reaction mixture was quickly foamed by the spontaneous heat, then gradually cooled to room temperature within 10 min. Finally, the HFCNs in the dark brown mixture were collected by dispersing in water for characterization or use.

Preparation of SFCNs. For the control experiment of synthesizing SFCNs, 1.5 g of P_2O_5 was first added into a centrifuge tube (5 mL). Then, 1 mL of acetic acid containing a very small amount of water (5 μL) was quickly injected into the centrifuge tube followed by quickly closing the lid. The centrifuge tube was vigorously shaken for 5 min, and a yellow-brown, sticky ball of PPA was obtained. This step is to avoid overheating of the acetic acid. The maximum temperature was measured to be about 90 °C by inserting a thermometer. Finally, SFCNs in the ball of PPA were dispersed in water and collected for further characterizations.

Synthesis of CdTe QDs. The green fluorescent CdTe QDs (λ_{em} = 515 nm) are prepared according to the literature.[53] Briefly, the precursor solution was prepared by mixing a solution of $CdCl_2$ (4 mM), Na_2TeO_3 (0.25 mM), and the buffer solution composed of 15 mM $Na_2B_4O_7$ and 15 mM citrate acid (pH = 7.2) in a one-neck flask and at room temperature. After vigorously stirring for 5 min, 20 mg of $NaBH_4$ powder was added rapidly to the precursor solution. The reactions proceeded for another 5 min, after which the flask was attached to a condenser and refluxed under open-air conditions for 45 min. Then, the reaction mixture was diluted with ethanol and centrifuged for 10 min. The precipitate was washed with water several times to remove the physical adsorbed ethanol and redispersed in 20 mM 4-(2-hydroxyethyl)-1-piperazineethanesulfonic acid (HEPES, pH = 7.4), which was directly used for cell imaging experiment. The concentration of CdTe QDs was determined by a previous method.[66]

MTT Assays and Cell Imaging. For the cell cytotoxicity test, HEK 293 cells were first plated on a Costar 96-well tissue-culture cluster and cultured at 37 °C with 5% CO_2 in air overnight to adhere cells onto the surface. The medium was then changed with 100 μL of fresh Dulbecco's modified Eagles' medium (10% fetal bovine serum) containing HFCNs or CdTe QDs, and the cells were allowed to grow for another 24 h. At least three parallel samples were performed in each group. Cells without treatment with HFCNs or CdTe QDs were taken as a control. After adding 10 μL of MTT reagent at a concentration of 5 mg/mL into each well, the cells were allowed to grow for another 4 h until a purple precipitate was visible. The medium was then removed, and 100 μL of dimethyl sulfoxide was added. The cluster was vibrated for 10 min to completely liberate the crystals. Finally, the absorption at 490 nm was measured with an EL808 ultra microplate reader (Bio TEK Instrument Inc.).

For the cell imaging experiment of HFCNs, HEK 293 cells (approximately 5×10^4 cells/well) were seeded in a 24-well plate and cultured at 37 °C. The filtered HFCN aqueous solution (50 μL, ~0.22 mg/mL) was mixed with the culture medium (500 μL) and then added to the wells. After incubation for 24 h, the HEK 293 cells were harvested using 0.25% trypsin/0.02% EDTA, washed three times with PBS (1 mL each time for three times), and kept in PBS for the optical imaging by a confocal microscope (Leica TCS SP2) with a 10× objective.

For CdTe QDs and FITC-labeled cells, CdTe QDs in HEPES buffer solution (40 μL, 2.8 mM) and FITC solution (40 μL, 0.01 mM) were mixed with the culture medium (450 mL), respectively, and then incubated for 4 h. Other procedures are exactly the same as that of HFCNs. It should be noted that the higher CdTe QD concentration and longer incubation time will significantly cause apoptosis due to the toxicity of CdTe. For Hoechst-labeled cells, Hoechst (10 μg/mL) was mixed with HEK 293 cells with slow shaking and incubated for 5 min, then washed three times with phosphate-buffered saline.

To ensure equal energy irradiation during the time-dependent comparison, all the fluorescence-labeled cell samples were excited by the same laser (λ_{ex} = 405 nm) with 50 mW power.

Two Extended Applications. *1. Fluorescent Watermark Ink.* The HFCNs ink was directly made from HFCN aqueous solution containing PPA. The HFCN aqueous solution was first neutralized to pH ≈ 7 by NaOH and then filtered through a filter membrane (220 nm). The filtrate was directly injected into a near-empty cartridge. The cartridge was used for printing until the exhaustion of initial ink and then refilled several times to exhaust the residual black ink until the diagram printed with HFCN ink on the paper could not be seen under ambient light (Figure 7B). It should be noted that filter paper was used as printing paper to avoid the influence of fluorescent additives in office printing papers.

2. Fluorescent Powder. The mixture of HFCNs in ethyl acetate solution and commercial silica powder was slowly stirred until dry under mild heat to obtain the fluorescent powder.

Characterization. The HFCNs were first extracted from aqueous solution by ethyl acetate. A drop of the HFCNs in ethyl acetate solution was carefully placed on the copper grid and dried at ambient conditions for transmission electron microscopy characterization. TEM and high-resolution TEM with electron dispersive X-ray spectrometry were performed on a Tecnai G_2 (FEI) instrument with an accelerating voltage of 200 kV. X-ray powder diffraction experiments were carried out by using a D/MAX 2500 V/PC X-ray diffractometer using Cu (40 kV, 40 mA) radiation, and the sample was prepared by drying the HFCNs in ethyl acetate solution. Infrared spectra were collected on a VERTEX Fourier transform infrared (FT-IR) spectrometer (Bruker). The sample in ethyl acetate was premixed with KBr powder, followed by grinding until the ethyl acetate was totally vaporized. The mixture was further dried in a vacuum drying oven at 80 °C for 12 h and then pressed into a disk for transmission infrared spectroscopy measurement. Raman spectra were obtained on a LabRAM HR800 Raman spectrometer (Jobin-Yvon, HORIBA Group, France) with 532 nm wavelength incident laser light. The ^{13}C nuclear magnetic resonance spectra of HFCNs dissolved in dimethyl sulfoxide-d_6 (DMSO-d_6) were recorded on a Bruker 600 M spectrometer. X-ray photoelectron spectroscopy measurements were performed by using an ESCALAB-MKII spectrometer (VG Co.) with Al Kα X-ray radiation as the X-ray source for excitation. Ethyl acetate solution containing HFCNs was washed and mixed with a large amount of water; then the mixture was boiled in an open beaker. Because of the azeotrope of ethyl acetate/water, the mixture finally removes ethyl acetate by vaporization, and some HFCNs in water solution were obtained for the cell imaging, the UV−vis measurement, and the dynamic light scattering experiment. UV−vis spectroscopy was carried out on a Cary 500 Scan UV−vis spectrophotometer (Varian, USA). The dynamic light scattering experiments and zeta potential measurements were conducted with a Zetasizer NanoZS (Malvern Instruments). The initial aqueous solution of HFCNs was directly centrifuged one time before the fluorescence measurements. Fluorescence measurements were carried out on a LS-55 luminescence spectrometer (Perkin-Elmer). The fluorescence spectra were recorded using 12.5 nm/10 nm slit widths.

SFCNs were treated with the same procedures if the characterization of the HFCNs needs SFCNs for the control.

Acknowledgment. This work was supported by the 973 Projects (2009CB930100 and 2010CB933600).

Supporting Information Available: Figure S1−11, supplemental results, and discussions. This material is available free of charge *via* the Internet at http://pubs.acs.org.

REFERENCES AND NOTES

1. Cao, L.; Wang, X.; Meziani, M. J.; Lu, F. S.; Wang, H. F.; Luo, P. J. G.; Lin, Y.; Harruff, B. A.; Veca, L. M.; Murray, D.; *et al.* Carbon Dots for Multiphoton Bioimaging. *J. Am. Chem. Soc.* **2007**, *129*, 11318–11319.
2. Yang, S. T.; Cao, L.; Luo, P. G. J.; Lu, F. S.; Wang, X.; Wang, H. F.; Meziani, M. J.; Liu, Y. F.; Qi, G.; Sun, Y. P. Carbon Dots for Optical Imaging *in Vivo*. *J. Am. Chem. Soc.* **2009**, *131*, 11308–11309.

3. Li, H. T.; He, X. D.; Kang, Z. H.; Huang, H.; Liu, Y.; Liu, J. L.; Lian, S. Y.; Tsang, C. H. A.; Yang, X. B.; Lee, S. T. Water-Soluble Fluorescent Carbon Quantum Dots and Photocatalyst Design. *Angew. Chem., Int. Ed.* **2010**, *49*, 4430–4434.
4. Cao, L.; Sahu, S.; Anilkumar, P.; Bunker, C. E.; Xu, J.; Fernando, K. A. S.; Wang, P.; Guliants, E. A.; Tackett, K. N.; Sun, Y. P. Carbon Nanoparticles as Visible-Light Photocatalysts for Efficient CO_2 Conversion and Beyond. *J. Am. Chem. Soc.* **2011**, *133*, 4754–4757.
5. Wang, F.; Chen, Y. H.; Liu, C. Y.; Ma, D. G. White Light-Emitting Devices Based on Carbon Dots' Electroluminescence. *Chem. Commun.* **2011**, *47*, 3502–3504.
6. Baker, S. N.; Baker, G. A. Luminescent Carbon Nanodots: Emergent Nanolights. *Angew. Chem., Int. Ed.* **2010**, *49*, 6726–6744.
7. Eda, G.; Lin, Y. Y.; Mattevi, C.; Yamaguchi, H.; Chen, H. A.; Chen, I. S.; Chen, C. W.; Chhowalla, M. Blue Photoluminescence from Chemically Derived Graphene Oxide. *Adv. Mater.* **2010**, *22*, 505–509.
8. Pan, D.; Zhang, J.; Li, Z.; Wu, M. Hydrothermal Route for Cutting Graphene Sheets into Blue-luminescent Graphene Quantum Dots. *Adv. Mater.* **2010**, *22*, 734–738.
9. Xu, X. Y.; Ray, R.; Gu, Y. L.; Ploehn, H. J.; Gearheart, L.; Raker, K.; Scrivens, W. A. Electrophoretic Analysis and Purification of Fluorescent Single-Walled Carbon Nanotube Fragments. *J. Am. Chem. Soc.* **2004**, *126*, 12736–12737.
10. Sun, Y. P.; Zhou, B.; Lin, Y.; Wang, W.; Fernando, K. A. S.; Pathak, P.; Meziani, M. J.; Harruff, B. A.; Wang, X.; Wang, H. F.; *et al*. Quantum-Sized Carbon Dots for Bright and Colorful Photoluminescence. *J. Am. Chem. Soc.* **2006**, *128*, 7756–7757.
11. Hu, S. L.; Sun, J.; Du, X. W.; Tian, F.; Jiang, L. The Formation of Multiply Twinning Structure and Photo Luminescence of Well-dispersed Nanodiamonds Produced by Pulsed-Laser Irradiation. *Diamond Relat. Mater.* **2008**, *17*, 142–146.
12. Hu, S. L.; Niu, K. Y.; Sun, J.; Yang, J.; Zhao, N. Q.; Du, X. W. One-Step Synthesis of Fluorescent Carbon Nanoparticles by Laser Irradiation. *J. Mater. Chem.* **2009**, *19*, 484–488.
13. Zhao, Q. L.; Zhang, Z. L.; Huang, B. H.; Peng, J.; Zhang, M.; Pang, D. W. Facile Preparation of Low Cytotoxicity Fluorescent Carbon Nanocrystals by Electrooxidation of Graphite. *Chem. Commun.* **2008**, 5116–5118.
14. Lu, J.; Yang, J. X.; Wang, J. Z.; Lim, A. L.; Wang, S.; Loh, K. P. One-Pot Synthesis of Fluorescent Carbon Nanoribbons, Nanoparticles, and Graphene by the Exfoliation of Graphite in Ionic Liquids. *ACS Nano* **2009**, *3*, 2367–2375.
15. Bottini, M.; Balasubramanian, C.; Dawson, M. I.; Bergamaschi, A.; Bellucci, S.; Mustelin, T. Isolation and Characterization of Fluorescent Nanoparticles from Pristine and Oxidized Electric Arc-Produced Single-Walled Carbon Nanotubes. *J. Phys. Chem. B* **2006**, *110*, 831–836.
16. Zhou, J. G.; Booker, C.; Li, R. Y.; Zhou, X. T.; Sham, T. K.; Sun, X. L.; Ding, Z. F. An Electrochemical Avenue to Blue Luminescent Nanocrystals from Multiwalled Carbon Nanotubes (MWCNTs). *J. Am. Chem. Soc.* **2007**, *129*, 744–745.
17. Qiao, Z. A.; Wang, Y. F.; Gao, Y.; Li, H. W.; Dai, T. Y.; Liu, Y. L.; Huo, Q. S. Commercially Activated Carbon as the Source for Producing Multicolor Photoluminescent Carbon Dots by Chemical Oxidation. *Chem. Commun.* **2010**, *46*, 8812–8814.
18. Dong, Y.; Zhou, N.; Lin, X.; Lin, J.; Chi, Y.; Chen, G. Extraction of Electrochemiluminescent Oxidized Carbon Quantum Dots from Activated Carbon. *Chem. Mater.* **2010**, *22*, 5895–5899.
19. Zheng, L. Y.; Chi, Y. W.; Dong, Y. Q.; Lin, J. P.; Wang, B. B. Electrochemiluminescence of Water-Soluble Carbon Nanocrystals Released Electrochemically from Graphite. *J. Am. Chem. Soc.* **2009**, *131*, 4564–4565.
20. Bourlinos, A. B.; Stassinopoulos, A.; Anglos, D.; Zboril, R.; Karakassides, M.; Giannelis, E. P. Surface Functionalized Carbogenic Quantum Dots. *Small* **2008**, *4*, 455–458.
21. Bourlinos, A. B.; Stassinopoulos, A.; Anglos, D.; Zboril, R.; Georgakilas, V.; Giannelis, E. P. Photoluminescent Carbogenic Dots. *Chem. Mater.* **2008**, *20*, 4539–4541.
22. Peng, H.; Travas-Sejdic, J. Simple Aqueous Solution Route to Luminescent Carbogenic Dots from Carbohydrates. *Chem. Mater.* **2009**, *21*, 5563–5565.
23. Li, H.; He, X.; Liu, Y.; Huang, H.; Lian, S.; Lee, S.-T.; Kang, Z. One-Step Ultrasonic Synthesis of Water-Soluble Carbon Nanoparticles with Excellent Photoluminescent Properties. *Carbon* **2011**, *49*, 605–609.
24. Zhang, J. C.; Shen, W. Q.; Pan, D. Y.; Zhang, Z. W.; Fang, Y. G.; Wu, M. H. Controlled Synthesis of Green and Blue Luminescent Carbon Nanoparticles with High Yields by the Carbonization of Sucrose. *New J. Chem.* **2010**, *34*, 591–593.
25. Pan, D. Y.; Zhang, J. C.; Li, Z.; Wu, C.; Yan, X. M.; Wu, M. H. Observation of pH-, Solvent-, Spin-, and Excitation-Dependent Blue Photoluminescence from Carbon Nanoparticles. *Chem. Commun.* **2010**, *46*, 3681–3683.
26. Wang, F.; Kreiter, M.; He, B.; Pang, S. P.; Liu, C. Y. Synthesis of Direct White-Light Emitting Carbogenic Quantum Dots. *Chem. Commun.* **2010**, *46*, 3309–3311.
27. Wang, F.; Pang, S.; Wang, L.; Li, Q.; Kreiter, M.; Liu, C. One-Step Synthesis of Highly Luminescent Carbon Dots in Noncoordinating Solvents. *Chem. Mater.* **2010**, *22*, 4528–4530.
28. Pan, D. Y.; Zhang, J. C.; Li, Z.; Wu, M. H. Hydrothermal Route for Cutting Graphene Sheets into Blue-Luminescent Graphene Quantum Dots. *Adv. Mater.* **2010**, *22*, 734–738.
29. Zhu, S.; Zhang, J.; Qiao, C.; Tang, S.; Li, Y.; Yuan, W.; Li, B.; Tian, L.; Liu, F.; Hu, R.; *et al*. Strongly Green-photoluminescent Graphene Quantum Dots for Bioimaging Applications. *Chem. Commun.* **2011**, *47*, 6858–6860.
30. Liu, H. P.; Ye, T.; Mao, C. D. Fluorescent Carbon Nanoparticles Derived from Candle Soot. *Angew. Chem., Int. Ed.* **2007**, *46*, 6473–6475.
31. Ray, S. C.; Saha, A.; Jana, N. R.; Sarkar, R. Fluorescent Carbon Nanoparticles: Synthesis, Characterization, and Bioimaging Application. *J. Phys. Chem. C* **2009**, *113*, 18546–18551.
32. Liu, R.; Wu, D.; Feng, X.; Müllen, K. Bottom-Up Fabrication of Photoluminescent Graphene Quantum Dots with Uniform Morphology. *J. Am. Chem. Soc.* **2011**, *133*, 15221–15223.
33. Yu, S. J.; Kang, M. W.; Chang, H. C.; Chen, K. M.; Yu, Y. C. Bright Fluorescent Nanodiamonds: No Photobleaching and Low Cytotoxicity. *J. Am. Chem. Soc.* **2005**, *127*, 17604–17605.
34. Chang, Y. R.; Lee, H. Y.; Chen, K.; Chang, C. C.; Tsai, D. S.; Fu, C. C.; Lim, T. S.; Tzeng, Y. K.; Fang, C. Y.; Han, C. C.; *et al*. Mass Production and Dynamic Imaging of Fluorescent Nanodiamonds. *Nat. Nanotechnol* **2008**, *3*, 284–288.
35. Liu, R. L.; Wu, D. Q.; Liu, S. H.; Koynov, K.; Knoll, W.; Li, Q. An Aqueous Route to Multicolor Photoluminescent Carbon Dots Using Silica Spheres as Carriers. *Angew. Chem., Int. Ed.* **2009**, *48*, 4598–4601.
36. Xiu, Y.; Gao, Q. A.; Li, G. D.; Wang, K. X.; Chen, J. S. Preparation and Tunable Photoluminescence of Carbogenic Nanoparticles Confined in a Microporous Magnesium-Aluminophosphate. *Inorg. Chem.* **2010**, *49*, 5859–5867.
37. Green, W. H.; Le, K. P.; Grey, J.; Au, T. T.; Sailor, M. J. White Phosphors from a Silicate-Carboxylate Sol-Gel Precursor That Lack Metal Activator Ions. *Science* **1997**, *276*, 1826–1828.
38. Zhu, H.; Wang, X. L.; Li, Y. L.; Wang, Z. J.; Yang, F.; Yang, X. R. Microwave Synthesis of Fluorescent Carbon Nanoparticles with Electrochemiluminescence Properties. *Chem. Commun.* **2009**, 5118–5120.
39. Michalet, X.; Pinaud, F. F.; Bentolila, L. A.; Tsay, J. M.; Doose, S.; Li, J. J.; Sundaresan, G.; Wu, A. M.; Gambhir, S. S.; Weiss, S. Quantum Dots for Live Cells, *in Vivo* Imaging, and Diagnostics. *Science* **2005**, *307*, 538–544.
40. Medintz, I. L.; Uyeda, H. T.; Goldman, E. R.; Mattoussi, H. Quantum Dot Bioconjugates for Imaging, Labelling and Sensing. *Nat. Mater.* **2005**, *4*, 435–446.
41. Gao, X. H.; Cui, Y. Y.; Levenson, R. M.; Chung, L. W. K.; Nie, S. M. In *Vivo* Cancer Targeting and Imaging with Semiconductor Quantum Dots. *Nat. Biotechnol.* **2004**, *22*, 969–976.
42. Derfus, A. M.; Chan, W. C. W.; Bhatia, S. N. Probing the Cytotoxicity of Semiconductor Quantum Dots. *Nano Lett.* **2004**, *4*, 11–18.
43. Kirchner, C.; Liedl, T.; Kudera, S.; Pellegrino, T.; Javier, A. M.; Gaub, H. E.; Stolzle, S.; Fertig, N.; Parak, W. J. Cytotoxicity of

Colloidal CdSe and CdSe/ZnS Nanoparticles. *Nano Lett.* **2005**, *5*, 331–338.
44. van Sark, W.; Frederix, P.; Van den Heuvel, D. J.; Gerritsen, H. C.; Bol, A. A.; van Lingen, J. N. J.; Donega, C. D.; Meijerink, A. Photooxidation and Photobleaching of Single CdSe/ZnS Quantum Dots Probed by Room-Temperature Time-Resolved Spectroscopy. *J. Phys. Chem. B* **2001**, *105*, 8281–8284.
45. Lu, Z. S.; Li, C. M. Quantum Dot-Based Nanocomposites for Biomedical Applications. *Curr. Med. Chem.* **2011**, *18*, 3516–3528.
46. Tan, W. B.; Huang, N.; Zhang, Y. Ultrafine Biocompatible Chitosan Nanoparticles Encapsulating Multi-Coloured Quantum Dots for Bioapplications. *J. Colloid Interface Sci.* **2007**, *310*, 464–470.
47. Yin, W.; Liu, H.; Yates, M. Z.; Du, H.; Jiang, F.; Guo, L.; Krauss, T. D. Fluorescent Quantum Dot-Polymer Nanocomposite Particles by Emulsification/Solvent Evaporation. *Chem. Mater.* **2007**, *19*, 2930–2936.
48. Yu, W. W.; Chang, E.; Falkner, J. C.; Zhang, J. Y.; Al-Somali, A. M.; Sayes, C. M.; Johns, J.; Drezek, R.; Colvin, V. L. Forming Biocompatible and Nonaggregated Nanocrystals in Water Using Amphiphilic Polymers. *J. Am. Chem. Soc.* **2007**, *129*, 2871–2879.
49. Nehilla, B. J.; Allen, P. G.; Desai, T. A. Surfactant-Free, Drug-Quantum-Dot Coloaded Poly(lactide-co-glycolide) Nanoparticles: Towards Multifunctional Nanoparticles. *ACS Nano* **2008**, *2*, 538–544.
50. Dembski, S.; Graf, C.; Kruger, T.; Gbureck, U.; Ewald, A.; Bock, A.; Ruhl, E. Photoactivation of CdSe/ZnS Quantum Dots Embedded in Silica Colloids. *Small* **2008**, *4*, 1516–1526.
51. Lu, Z. S.; Zhu, Z. H.; Zheng, X. T.; Qiao, Y.; Guo, J.; Li, C. M. Biocompatible Fluorescence-Enhanced ZrO_2-CdTe Quantum Dot Nanocomposite for *in vitro* Cell Imaging. *Nanotechnology* **2011**, *22*, 115604.
52. Lu, Z. S.; Hu, W. H.; Bao, H. F.; Qiao, Y.; Li, C. M. Interaction Mechanisms of CdTe Quantum Dots with Proteins Possessing Different Isoelectric Points. *MedChemComm* **2011**, *2*, 283–286.
53. Ying, E.; Li, D.; Guo, S.; Dong, S.; Wang, J. Synthesis and Bio-Imaging Application of Highly Luminescent Mercaptosuccinic Acid-Coated CdTe Nanocrystals. *Plos One* **2008**, *3*, e2222.
54. The *composite water* exists only as "water of composition" for the molecule form of two H atoms pulsed one O atom. P_2O_5 extracts the composite water to produce the hydrolysis product of P_2O_5. It is presented as the "composite water" to distinguish the free water.
55. Van Wazer, J. R. *Phosphorus and Its Compounds*; Interscience Publishers: New York, 1958; Vol. 1.
56. Bourbigot, S.; Lebras, M.; Delobel, R. Carbonization Mechanisms Resulting from Intumescence Association with the Ammonium Polyphosphate-Pentaerythritol Fire Retardant System. *Carbon* **1993**, *31*, 1219–1230.
57. Schrödter, K.; Bettermann, G.; Staffel, T.; Wahl, F.; Klein, T.; Hofmann, T. *Phosphoric Acid and Phosphates*; Wiley-VCH Verlag GmbH & Co. KGaA, 2000.
58. Neiss, T. G. Carbon-13 Nuclear Magnetic Resonance Spectroscopy. In *Encyclopedia of Analytical Chemistry*; John Wiley & Sons, Ltd., 2006.
59. Iijima, S. Helical Microtubules of Graphitic Carbon. *Nature* **1991**, *354*, 56–58.
60. Kang, Z. H.; Wang, E. B.; Gao, L.; Lian, S. Y.; Jiang, M.; Hu, C. W.; Xu, L. One-Step Water-Assisted Synthesis of High-Quality Carbon Nanotubes Directly from Graphite. *J. Am. Chem. Soc.* **2003**, *125*, 13652–13653.
61. Pelletier, M. J. *Analytical Applications of Raman Spectroscopy*; Wiley-Blackwell, 1999.
62. Ferrari, A. C.; Robertson, J. *Raman Spectroscopy in Carbons: from Nanotubes to Diamond*; The Royal Society: London, 2004.
63. Ferrari, A. C.; Rodil, S. E.; Robertson, J. Interpretation of Infrared and Raman Spectra of Amorphous Carbon Nitrides. *Phys. Rev. B* **2003**, *67*, 155306.
64. Ferrari, A. C.; Robertson, J. Interpretation of Raman Spectra of Disordered and Amorphous Carbon. *Phys. Rev. B* **2000**, *61*, 14095–14107.
65. Cancado, L. G.; Takai, K.; Enoki, T.; Endo, M.; Kim, Y. A.; Mizusaki, H.; Jorio, A.; Coelho, L. N.; Magalhaes-Paniago, R.; Pimenta, M. A. General Equation for the Determination of the Crystallite Size L_a of Nanographite by Raman Spectroscopy. *Appl. Phys. Lett.* **2006**, *88*, 163106.
66. Yu, W. W.; Qu, L. H.; Guo, W. Z.; Peng, X. G. Experimental Determination of the Extinction Coefficient of CdTe, CdSe, and CdS Nanocrystals. *Chem. Mater.* **2003**, *15*, 2854–2860.